A&A 566, A3 (2014)
DOI: 10.1051/0004-6361/201423711

Astronomy & Astrophysics

The virtual observatory service TheoSSA: Establishing a database of synthetic stellar flux standards

II. NLTE spectral analysis of the OB-type subdwarf Feige 110⋆,⋆⋆,⋆⋆⋆

T. Rauch[1], A. Rudkowski[1], D. Kampka[1], K. Werner[1], J. W. Kruk[2], and S. Moehler[3]

[1] Institute for Astronomy and Astrophysics, Kepler Center for Astro and Particle Physics, Eberhard Karls University, Sand 1, 72076 Tübingen, Germany
e-mail: rauch@astro.uni-tuebingen.de
[2] NASA Goddard Space Flight Center, Greenbelt MD 20771, USA
[3] European Southern Observatory, Karl-Schwarzschild-Str. 2, 85748 Garching, Germany

Received 26 February 2014 / Accepted 8 April 2014

ABSTRACT

Context. In the framework of the Virtual Observatory (VO), the German Astrophysical VO (GAVO) developed the registered service TheoSSA (Theoretical Stellar Spectra Access). It provides easy access to stellar spectral energy distributions (SEDs) and is intended to ingest SEDs calculated by any model-atmosphere code, generally for all effective temperatures, surface gravities, and elemental compositions. We will establish a database of SEDs of flux standards that are easily accessible via TheoSSA's web interface.
Aims. The OB-type subdwarf Feige 110 is a standard star for flux calibration. State-of-the-art non-local thermodynamic equilibrium stellar-atmosphere models that consider opacities of species up to trans-iron elements will be used to provide a reliable synthetic spectrum to compare with observations.
Methods. In case of Feige 110, we demonstrate that the model reproduces not only its overall continuum shape from the far-ultraviolet (FUV) to the optical wavelength range but also the numerous metal lines exhibited in its FUV spectrum.
Results. We present a state-of-the-art spectral analysis of Feige 110. We determined $T_{\rm eff} = 47\,250 \pm 2000$ K, $\log g = 6.00 \pm 0.20$, and the abundances of He, N, P, S, Ti, V, Cr, Mn, Fe, Co, Ni, Zn, and Ge. Ti, V, Mn, Co, Zn, and Ge were identified for the first time in this star. Upper abundance limits were derived for C, O, Si, Ca, and Sc.
Conclusions. The TheoSSA database of theoretical SEDs of stellar flux standards guarantees that the flux calibration of astronomical data and cross-calibration between different instruments can be based on models and SEDs calculated with state-of-the-art model-atmosphere codes.

Key words. standards – stars: abundances – stars: atmospheres – stars: individual: Feige 110 – subdwarfs – virtual observatory tools

1. Introduction

Feige 110 is a bright ($m_{\rm V} = 11.845 \pm 0.010$, Kharchenko & Roeser 2009), subluminous OB-star (type sdOB, Heber et al. 1984a; type sdO D,Vennes et al. 2011). It is widely used as a spectrophotometric standard star (e.g. Oke 1990; Turnshek et al. 1990; Bohlin et al. 1990). Since Feige 110 will be used as a reference star for the flux calibration of X-Shooter[1] (Vernet et al. 2011) observations from 3000 Å to 25 000 Å (Moehler et al. 2014), we decided to reanalyze its spectrum with state-of-the-art model-atmosphere techniques.

An early spectral analysis with approximate LTE[2], line-blanketed hydrogen model atmospheres yielded an effective temperature $T_{\rm eff} = 39\,000$ K and a surface gravity $\log(g/{\rm cm/s^2}) = 6.5$ (Newell 1973). Kudritzki (1976) showed that both, the consideration of deviations from non-LTE (NLTE) as well as of opacities of elements heavier than H, have a significant influence on the determination of $T_{\rm eff}$ and $\log g$ in an analysis of optical spectra (Table 1). Heber et al. (1984a) extended the analysis of Feige 110 to the ultraviolet (UV) wavelength range (IUE[3] observations, 1150 Å $\lesssim \lambda \lesssim$ 2000 Å) in addition to high-resolution optical spectra (4000 Å $\lesssim \lambda \lesssim$ 5100 Å) and derived $T_{\rm eff} = 40\,000^{+5000}_{-3000}$ K, $\log g = 5.0 \pm 0.3$, and He/H $= 0.03^{+0.03}_{-0.02}$ (by number) using H+He (with subsequent C+N+Si line-formation calculations) NLTE models.

With the FUSE[4] mission, the interstellar deuterium and oxygen column densities toward Feige 110 were measured. Friedman et al. (2002) used optical spectra and estimated the atmospheric parameters by comparison with a grid of synthetic NLTE model-atmosphere spectra (using TLUSTY to compute the stellar atmosphere model and SYNSPEC to generate the SED, Hubeny & Lanz 1995, just "TLUSTY" hereafter), that considered H and He. They achieved $T_{\rm eff} = 42\,300 \pm 1000$ K, $\log g = 5.95 \pm 0.15$, and He/H $= 0.011 \pm 0.005$. With the higher

⋆ Based on observations with the NASA/ESA *Hubble* Space Telescope, obtained at the Space Telescope Science Institute, which is operated by the Association of Universities for Research in Astronomy, Inc., under NASA contract NAS5-26666.
⋆⋆ Based on observations made with the NASA-CNES-CSA Far Ultraviolet Spectroscopic Explorer.
⋆⋆⋆ Table 2, Figs. 3 and 7 are available in electronic form at http://www.aanda.org
[1] http://www.eso.org/sci/facilities/paranal/instruments/xshooter.html
[2] Local thermodynamic equilibrium.
[3] International Ultraviolet Explorer.
[4] Far Ultraviolet Spectroscopic Explorer.

Table 1. $T_{\rm eff}$ and $\log g$ of Feige 110 determined by Kudritzki (1976).

LTE		NLTE		He/H
$T_{\rm eff}$/K	$\log(g/{\rm cm/s^2})$	$T_{\rm eff}$/K	$\log(g/{\rm cm/s^2})$	
42 600	6.3	44 600	5.9	0.1
42 400	6.5	42 700	6.4	1.0

Notes. He/H gives his models' abundance ratio by number.

$\log g$ (in agreement with Kudritzki 1976), their spectroscopic distance of $d = 288 \pm 43$ pc agreed with the HIPPARCOS[5] parallax distance of $d = 179^{+265}_{-67}$ pc.

In the following, we describe our analysis in detail. In Sect. 2, we give some remarks on the observations. Then, we introduce our models and the considered atomic data (Sect. 3) and start with a preliminary analysis (Sect. 4) of the optical spectrum based on H+He models followed by a highly sophisticated analysis with metal-line blanketed models (Sect. 5). We summarize our results and conclude in Sect. 6.

2. Observations

Our main optical spectrum is a median of 19 X-Shooter observations, taken between 26 October 2011 and 5 July 2012 with a 5″ slit (the seeing was below 1″ during the observations) and an exposure time of 120 s each. The achieved resolving power was $R = \lambda/\Delta\lambda \approx 4800$. All spectra were extracted with ESO's standard pipeline-reduction software (with the actual version at the time of the respective observation). Heliocentric correction and correction to an airmass =0 were applied. In addition, we used optical HST/STIS[6] spectra (ObsIds O40801010 and O40801030 co-added) from the archive for the determination of the interstellar reddening.

Our far-ultraviolet (FUV) spectrum consists of two observations of Feige 110 that were performed by FUSE, both in June 2000 and both through the LWRS spectrograph aperture. The dataset IDs were M1080801 and P1044301, with exposure times of 6.2 ks and 21.8 ks, respectively. Alignment of the four FUSE telescope channels was excellent throughout both observations, with RMS exposure-to-exposure variations in flux under 0.5% in all channels. The processing of individual exposures to produce a combined spectrum spanning 905–1188 Å was the same as that described for G191−B2B in Rauch et al. (2013) and won't be repeated here. The signal to noise per 0.013 Å pixel in the continuum for the combined spectrum is typically 80:1 shortward of 1000 Å and 120:1 longward of 1000 Å. Approximately 37% of the exposure time was obtained during orbital night. Comparison of the spectra obtained during day and night portions of the orbit found a discernible difference only in the cores of Ly β and Ly γ. Only the night data were used for these spectral regions. Weak airglow emission was still present at Ly β during orbital night, but the affected pixels had no impact on the analysis of the stellar spectrum.

Additional UV spectra were retrieved from MAST. We used all available low-resolution IUE spectra (SWP03737, SWP20091, SWP21888, SWP21890, SWP21891, SWP21892, LWP01913, LWP01914, LWP01915, LWP02505, LWP02506, LWP02507, LWP02508, and LWR11785 co-added) and an HST/STIS spectrum (ObsId OBIE01010, exposure time 1734.2 s, start time 2010-12-12 08:10:54 UT, grating G140M, 1191 Å $\lesssim \lambda \lesssim$ 1246 Å, aperture 52″ × 0.″05, resolution = 0.1 Å).

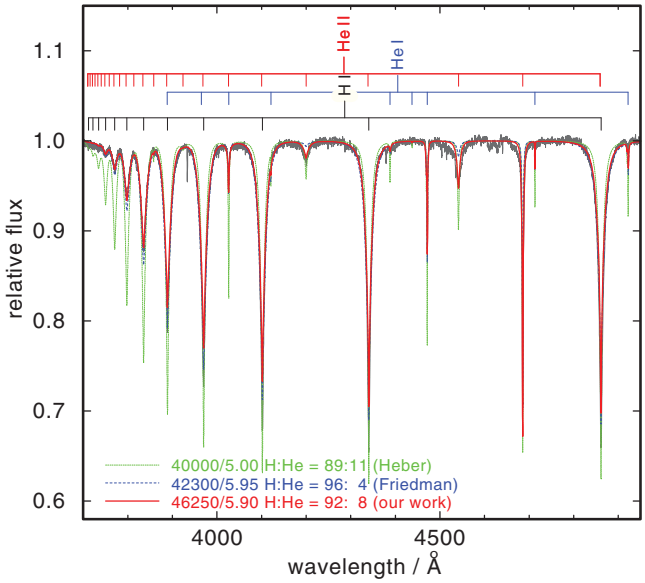

Fig. 1. Comparison of three synthetic spectra with our optical observation of Feige 110. $T_{\rm eff}$, $\log g$, and the H:He ratio by mass are indicated.

3. Model atmospheres and atomic data

For our model-atmosphere calculations, we use the Tübingen NLTE model-atmosphere package[7] (Werner et al. 2003; Rauch & Deetjen 2003), that assumes a plane-parallel geometry and considers opacities of elements from H to Ni (Rauch 1997, 2003). The models are in hydrostatic and radiative equilibrium. TMAP was successfully used for many spectral analyses of hot, compact stars (e.g. Rauch et al. 2007, 2013; Wassermann et al. 2010; Klepp & Rauch 2011; Ziegler et al. 2012).

The model atoms used in our model-atmosphere calculations were either retrieved from the Tübingen model-atom database[8] or compiled via the registered Virtual Observatory (VO) tool TIRO[9] that uses Kurucz's atomic data[10] and line lists (Kurucz 1991, 2009, 2011, and priv. comm.). Table 2 shows the statistics of our model atoms.

4. Preliminary analysis

For a preliminary analysis, or verification of basic previous results, we employ the registered VO service TheoSSA[11] and the related registered VO tool TMAW[12], to download precalculated synthetic spectral energy distributions (SEDs) or to calculate individual SEDs, respectively (cf. Rauch et al. 2013). Figure 1 shows a comparison of SEDs with model parameters of Heber et al. (1984a), Friedman et al. (2002), and of this work with the observed optical spectrum. The Balmer decrement is a sensitive indicator of $\log g$ (e.g. Rauch et al. 1998),

[5] http://www.rssd.esa.int/index.php?project=HIPPARCOS
[6] *Hubble* Space Telescope/Space Telescope Imaging Spectrograph.
[7] TMAP, http://astro.uni-tuebingen.de/~TMAP
[8] TMAD, http://astro.uni-tuebingen.de/~TMAD
[9] Tübingen iron-opacity interface.
[10] http://kurucz.harvard.edu/atoms.html
[11] Theoretical Stellar Spectra Access, http://dc.g-vo.org/theossa
[12] Tübingen Model-Atmosphere WWW Interface.

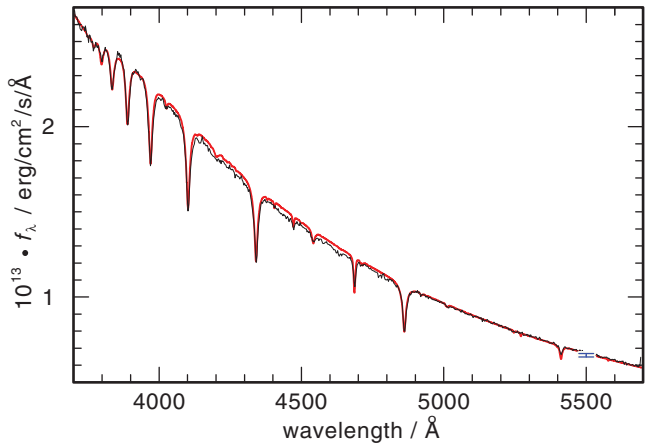

Fig. 2. Comparison of the optical HST/STIS observation with our final model SED. The synthetic spectrum is convolved with a Gaussian ($FWHM$ = 5 Å) to match the resolution of the observation. The error bar indicates the visual brightness (m_V = 11.847 ± 0.010).

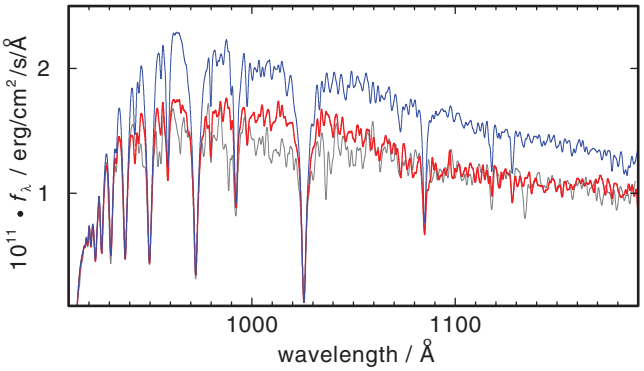

Fig. 4. FUSE observation of Feige 110 (gray) compared with two synthetic spectra calculated from our final model (thin, blue in the online version: with Kurucz's POS lines; thick, red: with Kurucz's LIN lines). All spectra are convolved with a Gaussian ($FWHM$ = 1 Å) for clarity.

and we derive $\log g = 5.90 \pm 0.20$. At this $\log g$, the He I/He II ionization equilibrium, i.e. the measured equivalent-width ratio of He I and He II lines, is well reproduced by our model at $T_{\rm eff}$ = 46 250 ± 2000 K. The He line strengths are matched at a photospheric He abundance of 8±2% by mass. Although the theoretical H and He line profiles agree well with the observation, the central depressions are not matched perfectly. This may be a hint that a weak Balmer-line problem (cf. Napiwotzki & Rauch 1994; Rauch 2000) exists because metal opacities are neglected. For the same reason, our synthetic H+He SEDs are not suitable for an analysis of the H I Lyman lines in FUV spectrum. Fully metal-line blanketed model-atmospheres are mandatory for this purpose (Sect. 5). However, from our derived $T_{\rm eff}$, we are well in the parameter range where no deviation between H I Lyman- and Balmer-line analysis is expected (Good et al. 2004, their Fig. 4).

We adopt our derived $T_{\rm eff}$ and $\log g$ values, that also reproduce well the HST/STIS observation (Fig. 2), for our further analysis and will verify them with our final, fully metal-line blanketed model.

Within error limits, our preliminary values agree well with those of Friedman et al. (2002). Only $\Delta T_{\rm eff}$ = ±1000 from their χ^2 fit appears to be too optimistic. It is worthwhile to note, that the result of Kudritzki (1976, Table 1, his lower He abundance model) is relatively close to our result.

5. Line identification and detailed analysis

Friedman et al. (2002) identified photospheric lines from N III–V, S VI, Cr IV–V, Fe III–IV, and Ni IV in the FUSE observation. Their SED calculation (SYNSPEC, Hubeny & Lanz 1995) included all elements from H to Zn, all with solar abundances but He (1.3×10^{-1} times solar), C ($\approx 4 \times 10^{-6}$ times solar), Si ($\approx 2 \times 10^{-7}$ times solar), and Cr (≈21 times solar).

We decided to include H, He, C, N, O, Si, P, S, Ca, Sc, Ti, V, Cr, Mn, Fe, Co, Ni, Zn, and Ge in our calculations. Figure 3 shows the ionization fractions of these elements. For the iron-group elements (here Ca–Ni), the dominant ionization stages are IV–V. All SEDs that were calculated for this analysis are available via TheoSSA.

For the line identification in the FUSE wavelength range (905–1188 Å), it was necessary to determine the stellar continuum flux precisely. We started with a measurement of the interstellar neutral hydrogen column density. From Ly α in the STIS spectrum and the higher members of the Lyman series in the FUSE spectrum, we determined $n_{\rm H\,I} = 1.8 \pm 0.8 \times 10^{20}$ cm^{-2} in agreement with Friedman et al. (2002, $n_{\rm H\,I} = 1.4 \pm 0.5 \times 10^{20}$ cm^{-2} determined from the high-resolution IUE spectrum SWP15270). To measure the interstellar reddening, we normalized our synthetic spectrum to the 2MASS H brightness because the interstellar reddening is negligible there and adjusted E_{B-V} to match the IUE, STIS, and FUSE flux levels. Our result is $E_{B-V} = 0.027 \pm 0.007$. This very low value is in agreement with the absence of the 2175 Å bump in the IUE LWP spectra (Sect. 2). The Galactic reddening law of Liszt (2014a,b, valid for $0.015 \lesssim E_{B-V} \lesssim 0.075$ and $|b| \geq 20°$), $N_{\rm H\,I}/E_{B-V} = 8.3{\times}10^{21}$ cm^{-2}mag^{-1}, predicts $0.012 \leq E_{B-V} \leq 0.031$ in agreement with our value.

The comparison of our models to the FUSE observations shows that we can reproduce well the observed flux level (Fig. 4), if we include all the lines from Kurucz's LIN lists (Sect. 3). These include laboratory-measured lines with "good wavelengths" as well as theoretical lines[13]. The lines with good wavelengths are presented in Kurucz's POS lists. Unfortunately, the ratio of LIN to POS lines is about 100 and thus, most line wavelengths are uncertain. Moreover, the continuum flux of the POS-line spectrum appears artificially high compared to the LIN spectrum due to the neglected line opacity (Fig. 5).

The line-identification process is easy (the comparison of two SEDs calculated from our final model where the oscillator strengths of one individual atom/ion was artificially reduced for one SED). It enabled us to unambiguously identify hundreds of lines of N, O, P, S, Ti, V, Cr, Mn, Fe, Mn, Ni, Zn, and Ge.

Our metal-line blanketed models have a different atmospheric structure compared to the H-He models that were used in the preliminary determination of $T_{\rm eff}$ = 46 250 K and $\log g = 5.90$ (Sect. 4). Figure 6 shows the typical surface-cooling ($\log m \lesssim -2.5$) and backwarming effects ($\log m \gtrsim -2.5$), that are an impact of the additionally considered metal opacities. A detailed evaluation of the optical spectrum shows that slightly higher $T_{\rm eff}$ = 47 250 K and $\log g = 6.00$ values are necessary to reproduce the He I/He II ionization equilibrium and the observed H I, He I, and He II line profiles best.

The abundance analysis follows a standard procedure. Identified lines are reproduced by an abundance adjustment of

[13] Kurucz's LIN lists are used in our model-atmosphere calculations.

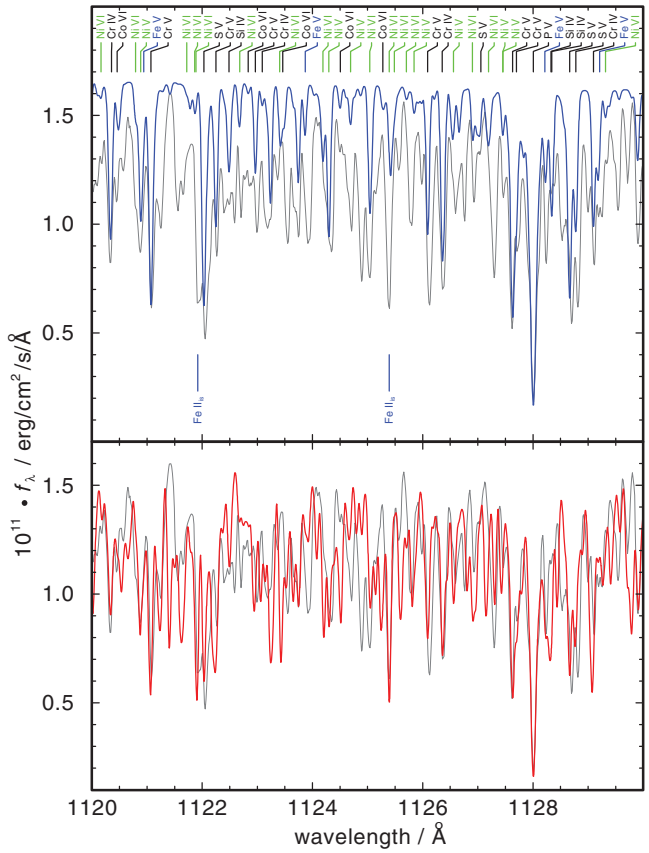

Fig. 5. Same as Fig. 4, for a section of the FUSE observation (*top panel*: POS, *bottom panel*: LIN). The POS lines are identified (in black, Fe and Ni lines in blue and green for clarity, respectively) at the top of the top panel. Lines of interstellar origin are marked in blue (with subscript "is") at the bottom of the top panel. The synthetic spectra are convolved with a Gaussian (*FWHM* = 0.06 Å) to match FUSE's resolution.

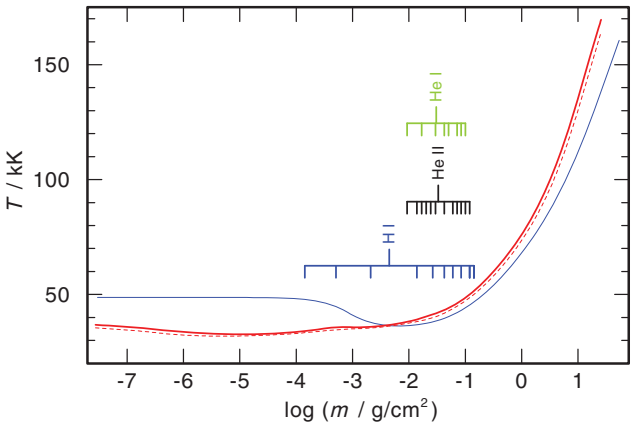

Fig. 6. Temperature structure of our H+He model (thin, blue line: $T_{\rm eff}$ = 46 250 K, log g = 5.90), a metal-line blanketed model with the same $T_{\rm eff}$ and log g (dashed, red), and of our final model (thick, red: $T_{\rm eff}$ = 47 250 K, log g = 6.00). The formation depths of the lines cores of optical lines of H I (Hα is the most outside), He I, and He II are shown.

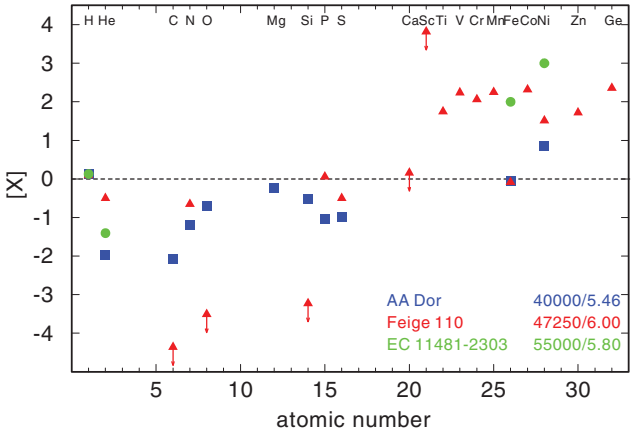

Fig. 8. Comparison of the determined photospheric abundances (arrows indicate upper limits) of the three OB-type subdwarfs AA Dor (Klepp & Rauch 2011), EC 11481−2303 (Rauch et al. 2010), and Feige 110. Their $T_{\rm eff}$ and log g are shown in the legend.

the respective species. For elements with no lines identified, we increased the abundances until their line-detection limit. The optical spectrum was used to further constrain the upper limit because lines of lower ionization stages, that are not observed, appear there at too-high abundances in the synthetic spectrum. Table 3 summarizes the lines that were used and the derived abundances.

To identify ISM[14] absorption lines in the FUSE observation (cf. Friedman et al. 2002) and to judge the contamination of photospheric lines, we follow our standard procedure and model the stellar spectrum simultaneously with the ISM line absorption (e.g., Rauch et al. 2013). We modeled the latter with the program OWENS (Hébrard et al. 2002; Hébrard & Moos 2003), that considers different clouds with individual radial and turbulent velocities, temperatures, column densities and chemical compositions. Lines are represented by Voigt profiles. The best fit is determined via a χ^2 method. Our ISM model includes lines of H_2 (J = 0–9), H I, D I, C II–III, N I–II, O I, Si I–II, P II, Ar I, and Fe II. Our results for D I and O I are consistent with those of Friedman et al. (2002).

The complete FUSE observation is compared (including line identifications) with our final model in Fig. 7.

[14] Interstellar medium.

6. Results and conclusions

We performed a comprehensive spectral analysis of Feige 110, based on observations from the FUV to the optical wavelength range. We determined $T_{\rm eff}$ = 47 250 ± 2000 K and log g = 6.00 ± 0.20. The ionization equilibria of He I/He II, N III/N IV/N V, P IV/P V, S IV/S V/S VI, Ti IV/Ti V, V IV/V V, Cr IV/Cr V/Cr VI, Mn V/Mn VI, Fe V/Fe VI, Co V/Co VI, and Ni V/Ni VI are well reproduced with these values. The photospheric abundances were determined based on the FUSE and optical observations (Table 3). Figure 8 shows a comparison of the photospheric abundances patterns of three hot O(B)-type subdwarfs. While the intermediate-mass metals are solar or subsolar in all these stars, the iron-group elements but Fe have strongly super-solar values. An exception is Fe in AA Dor and EC 11481−2303, that appears to be solar. Neither this Fe peculiarity nor the extremely low C and Si abundances in Feige 110 can be explained.

The position of Feige 110 in the $T_{\rm eff}$−log g plane shows that it is located directly on the He main sequence (Fig. 9). Feige 110 belongs, like AA Dor or EC 11481−2303, to the

Table 3. Strategic lines and determined element abundances (mass fraction, error ±0.2 dex).

Element	Analyzed lines	Abundance	[X]
H	optical H I lines	9.12×10^{-1}	0.00
He	optical He I–II lines	7.93×10^{-2}	−0.50
C	C III $\lambda\lambda$ 1174–1176 Å	$<1.04\times10^{-7}$	<−4.36
	C IV $\lambda\lambda$ 1118.41, 1122.49, 1168–1169 Å		
N	N III $\lambda\lambda$ 1182.97, 1183.03, 1184.51, 1184.57 Å	1.56×10^{-4}	−0.65
	N III $\lambda\lambda$ 3998.63, 4003.58, 4379.11, 4510.91, 4514.86, 4634.14, 4640.64 Å		
	N IV $\lambda\lambda$ 921.99, 922.52, 923.06, 923.22, 923.68, 924.28 Å		
	N V $\lambda\lambda$ 1238.82, 1242.80 Å		
O	O III λ 1153.78 Å	$<1.78\times10^{-6}$	<−3.51
	O IV $\lambda\lambda$ 921.30, 921.36, 923.37, 923.43 Å		
Si	Si III λ 1113.23 Å	$<3.96\times10^{-7}$	<−3.23
	Si IV λ 1122.49 Å		
P	P IV $\lambda\lambda$ 1025.56, 1028.09, 1030.51, 1030.51, 1033.11, 1035.52 Å	6.67×10^{-6}	0.06
	P V $\lambda\lambda$ 1117.98, 1128.01 Å		
S	S IV $\lambda\lambda$ 1062.66, 1072.97, 1073.52, 1098.93, 1099.48 Å	9.77×10^{-5}	−0.50
	S V $\lambda\lambda$ 1039.92, 1122.03, 1128.67, 1128.78 Å		
	S VI $\lambda\lambda$ 933.38, 944.52 Å		
Ca	optical Ca IV lines	$<9.27\times10^{-5}$	<0.16
Sc	Sc IV λ 931.42 Å	$<3.08\times10^{-4}$	<3.82
	Sc V $\lambda\lambda$ 939.40, 944.04 Å		
Ti	optical Ti IV lines, Ti IV λ 1183.63 Å	1.77×10^{-4}	2.24
	Ti V $\lambda\lambda$ 1153.28, 1163.52 Å		
V	V IV λ 1131.25 Å	5.50×10^{-5}	2.06
	V V $\lambda\lambda$ 978.16, 1142.74, 1157.58 Å		
Cr	many Cr IV–VI lines in the FUV, e.g.	1.92×10^{-3}	2.06
	Cr IV $\lambda\lambda$ 1043.46, 1065.26, 1072.10, 1096.64, 1126.35 Å		
	Cr V $\lambda\lambda$ 1031.10, 1035.04, 1042.55, 1045.04, 1060.65 Å		
	Cr VI λ 957.01 Å		
Mn	Mn V $\lambda\lambda$ 1040.04, 1043.65, 1048.63, 1049.43, 1055.98, 1062.49, 1172.06 Å	1.92×10^{-3}	2.25
	Mn VI $\lambda\lambda$ 1081.09, 1113.58 Å		
Fe	many Fe V–VI lines in the FUV, e.g.	1.08×10^{-3}	−0.08
	Fe V $\lambda\lambda$ 1002.87, 1015.33, 1020.36 Å		
	Fe VI $\lambda\lambda$ 1000.93, 1167.70 Å		
Co	many Co V–VI lines in the FUV, e.g.	8.72×10^{-4}	2.32
	Co V $\lambda\lambda$ 1179.59, 1183.91, 1184.60 Å		
	Co VI $\lambda\lambda$ 1133.71, 1142.77, 1150.23, 1169.55, 1175.36 Å		
Ni	many Ni V–VI lines in the FUV, e.g.	2.28×10^{-3}	1.51
	Ni V $\lambda\lambda$ 1124.30, 1178.92 Å		
	Ni VI $\lambda\lambda$ 1000.39, 1157.55, 1159.00, 1178.37 Å		
Zn	Zn V $\lambda\lambda$ 1116.84, 1120.33, 1158.76 Å	9.08×10^{-5}	1.72
Ge	Ge V $\lambda\lambda$ 1016.67, 1069.13, 1072.66, 1116.95, 1165.26 Å	5.38×10^{-5}	2.36

Notes. [X] = log (abundance/solar abundance) of species X (solar values from Asplund et al. 2009).

hottest post-EHB[15] stars. From a comparison to post-EHB tracks (Dorman et al. 1993), we can extrapolate a stellar mass of $M = 0.469\pm0.001\,M_\odot$. With $R = \sqrt{GM/g}$ (G is the gravitational constant), we calculated the stellar radius of $R = 0.114^{+0.030}_{-0.024}\,R_\odot$.

We determined the distance of Feige 110 following the flux calibration of Heber et al. (1984b) for $\lambda_{\rm eff}$ = 5454 Å,

$$d_{\rm spec} = 7.11\times10^4 \cdot \sqrt{H_\nu \cdot M \cdot 10^{0.4\,m_{\rm V_0}-\log g}}\ {\rm pc}\,, \qquad (1)$$

with $m_{\rm V_o} = m_{\rm V} - 2.175c$, $c = 1.475E_{\rm B-V}$, and the Eddington flux $H_\nu = 7.24\pm0.37\times10^{-4}$ erg/cm^2/s/Hz at $\lambda_{\rm eff}$ of our final model atmosphere. We used $E_{B-V} = 0.027\pm0.007$ (Sect. 4), $M = 0.469\pm+0.001\,M_\odot$, and $m_{\rm V} = 11.847\pm0.010$ (Kharchenko & Roeser 2009) and derived a distance of $d_{\rm spec} = 297^{+62}_{-77}$ pc and a height below the Galactic plane of $z = 255^{+53}_{-66}$ pc. This distance is about a factor of three larger than the new HIPPARCOS parallax-measurement reduction (van Leeuwen 2007, HIP115195, $\pi = 9.76\pm3.44$ mas) of $d_{\rm parallax} = 102.46^{+55.78}_{-26.69}$ pc. Interestingly, the older HIPPARCOS measurement published by Perryman et al. (1997, $\pi = 5.59\pm3.34$ mas, $d_{\rm parallax} = 178.89^{+265.55}_{-66.91}$ pc) deviates from this new value by a factor of almost two and would be in agreement with our spectroscopic distance within error limits.

The discrepancy between spectroscopic and parallax distances is a significant problem. $\log g$ cannot be higher by about 0.5 to achieve a distance agreement, because the spectral lines in the models appear too broad and too shallow. This apparently is not a problem of our TMAP code, because Friedman et al. (2002, $d_{\rm spec} = 288\pm43$ pc) used the TLUSTY code and encountered the same problem. Similar discrepancies are reported by Rauch et al. (2007, for LSV+46°21 with TMAP: $d_{\rm spec} = 224^{+46}_{-58}$ pc vs. $d_{\rm parallax} = 129^{+6}_{-5}$ pc) and by Latour et al. (2013, for BD+28°4211 with TLUSTY, $T_{\rm eff}$ = 82 000 K, $\log g$ = 6.2, and an assumed $M = 0.5\,M_\odot$: $d_{\rm spec} = 157$ pc (no error estimate given) vs. $d_{\rm parallax} = 92^{+13}_{-11}$ pc).

Latour et al. (2013) mentioned that a relatively high $\log g$ value and/or a low mass may be the solution and since they

[15] Extended horizontal branch.

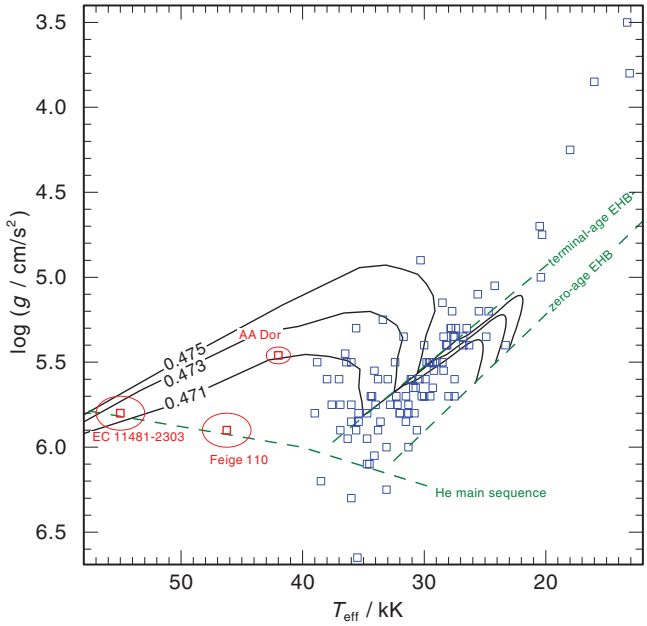

Fig. 9. Location of Feige 110 in the $T_{\rm eff}-\log g$ plane compared to sdBs and sdOBs from Edelmann (2003), Rauch et al. (2010, EC 11481−2303), and Klepp & Rauch (2011, AA Dor). Post-EHB tracks from Dorman et al. (1993, $Y_{\rm HB} = 0.288$, labeled with the respective stellar masses in $M_\odot$) are also shown. Their start and kink points are used to illustrate the location of the zero-age and terminal-age EHB for this He composition. The He main sequence is taken from Paczyński (1971).

regard the HIPPARCOS measurement as fully reliable and their TLUSTY results reasonably reliable, the mass of BD+28°4211 must be much less than the canonical post-EHB mass of about $0.5\,M_\odot$. For their $d_{\rm parallax}/d_{\rm spec} = 0.59$, the mass has to be about $0.17\,M_\odot$. In case of Feige 110, with $d_{\rm parallax}/d_{\rm spec} = 0.31$, the mass has to be about $0.10\,M_\odot$. In both cases, the mass can be higher, if $\log g$ is higher. Thus, since $\log g$ is also the main error source in the spectroscopic distance (Eq. (1)), one might speculate about the applied broadening theory for lines that are used to determine $\log g$. For the relevant H I and He II lines (linear Stark effect), TMAP as well as TLUSTY use the same data of Tremblay & Bergeron (2009) and Schöning & Butler (1989), respectively. However, all the narrow metal lines (e.g. of the iron-group element) in the UV, that are broadened by the quadratic Stark effect, cannot be reproduced at a much higher $\log g$. To summarize, the distance discrepancy is as yet unexplained.

The analysis of the FUV spectrum has shown that the lack of reliably measured wavelengths of lines of the iron-group elements (Ca−Ni) and of elements heavier than Ni hampers the line-identification. Efforts in this field in the near future are highly desirable.

The established database of spectrophotometric standard stars in TheoSSA was extended by the OB-type subdwarf Feige 110. The successfully launched *Gaia*[16] mission will provide accurate parallax measurements for spectrophotometric standard stars. This will strengthen the importance of a VO-compliant database like TheoSSA that provides easy access to the best synthetic spectra calculated for these stars.

Acknowledgements. T.R. is supported by the German Aerospace Center (DLR, grant 05 OR 1301). The GAVO project at Tübingen has been supported by the Federal Ministry of Education and Research (BMBF, grants 05 AC 6 VTB, 05 AC 11 VTB). This work used the profile-fitting procedure OWENS developed by M. Lemoine and the FUSE French Team. This research has made use of the SIMBAD database, operated at the CDS, Strasbourg, France. This research has made use of NASA's Astrophysics Data System. Some of the data presented in this paper were obtained from the Mikulski Archive for Space Telescopes (MAST). STScI is operated by the Association of Universities for Research in Astronomy, Inc., under NASA contract NAS5-26555. Support for MAST for non-HST data is provided by the NASA Office of Space Science via grant NNX09AF08G and by other grants and contracts. The TIRO service (http://astro-uni-tuebingen.de/~TIRO) used to calculate opacities for this paper was constructed as part of the activities of the German Astrophysical Virtual Observatory. The TMAW service (http://astro-uni-tuebingen.de/~TMAW) used to calculate theoretical spectra for this paper was constructed as part of the activities of the German Astrophysical Virtual Observatory.

References

Asplund, M., Grevesse, N., Sauval, A. J., & Scott, P. 2009, ARA&A, 47, 481
Bohlin, R. C., Harris, A. W., Holm, A. V., & Gry, C. 1990, ApJS, 73, 413
Dorman, B., Rood, R. T., & O'Connell, R. W. 1993, ApJ, 419, 596
Edelmann, H. 2003, Dissertation, University Erlangen-Nuremberg, Germany
Friedman, S. D., Howk, J. C., Chayer, P., et al. 2002, ApJS, 140, 37
Good, S. A., Barstow, M. A., Holberg, J. B., et al. 2004, MNRAS, 355, 1031
Heber, U., Hamann, W.-R., Hunger, K., et al. 1984a, A&A, 136, 331
Heber, U., Hunger, K., Jonas, G., & Kudritzki, R. P. 1984b, A&A, 130, 119
Hébrard, G., & Moos, H. W. 2003, ApJ, 599, 297
Hébrard, G., Friedman, S. D., Kruk, J. W., et al. 2002, Planet. Space Sci., 50, 1169
Hubeny, I., & Lanz, T. 1995, ApJ, 439, 875
Kharchenko, N. V., & Roeser, S. 2009, VizieR Online Data Catalog: I/280
Klepp, S., & Rauch, T. 2011, A&A, 531, L7
Kudritzki, R.-P. 1976, A&A, 52, 11
Kurucz, R. L. 1991, in Stellar Atmospheres – Beyond Classical Models, eds. L. Crivellari, I. Hubeny, & D. G. Hummer, NATO ASIC Proc. 341, 441
Kurucz, R. L. 2009, in AIP Conf. Ser. 1171, eds. I. Hubeny, J. M. Stone, K. MacGregor, & K. Werner, 43
Kurucz, R. L. 2011, Canadian J. Phys., 89, 417
Latour, M., Fontaine, G., Chayer, P., & Brassard, P. 2013, ApJ, 773, 84
Liszt, H. 2014a, ApJ, 783, 17
Liszt, H. 2014b, ApJ, 780, 10
Moehler, S., Modigliani, A., Freudling, W., et al. 2014, A&A, in press, DOI: 10.1051/0004-6361/201423790
Napiwotzki, R., & Rauch, T. 1994, A&A, 285, 603
Newell, E. B. 1973, ApJS, 26, 37
Oke, J. B. 1990, AJ, 99, 1621
Paczyński, B. 1971, Acta Astron., 21, 1
Perryman, M. A. C., Lindegren, L., Kovalevsky, J., et al. 1997, A&A, 323, L49
Rauch, T. 1997, A&A, 320, 237
Rauch, T. 2000, A&A, 356, 665
Rauch, T. 2003, A&A, 403, 709
Rauch, T., & Deetjen, J. L. 2003, in Stellar Atmosphere Modeling, eds. I. Hubeny, D. Mihalas, & K. Werner, ASP Conf. Ser., 288, 103
Rauch, T., Dreizler, S., & Wolff, B. 1998, A&A, 338, 651
Rauch, T., Ziegler, M., Werner, K., et al. 2007, A&A, 470, 317
Rauch, T., Werner, K., & Kruk, J. W. 2010, Ap&SS, 329, 133
Rauch, T., Werner, K., Bohlin, R., & Kruk, J. W. 2013, A&A, 560, A106
Schöning, T., & Butler, K. 1989, A&AS, 78, 51
Tremblay, P.-E., & Bergeron, P. 2009, ApJ, 696, 1755
Turnshek, D. A., Bohlin, R. C., Williamson, II, R. L., et al. 1990, AJ, 99, 1243
van Leeuwen, F. 2007, A&A, 474, 653
Vennes, S., Kawka, A., & Németh, P. 2011, MNRAS, 410, 2095
Vernet, J., Dekker, H., D'Odorico, S., et al. 2011, A&A, 536, A105
Wassermann, D., Werner, K., Rauch, T., & Kruk, J. W. 2010, A&A, 524, A9
Werner, K., Deetjen, J. L., Dreizler, S., et al. 2003, in Stellar Atmosphere Modeling, eds. I. Hubeny, D. Mihalas, & K. Werner, ASP Conf. Ser., 288, 31
Ziegler, M., Rauch, T., Werner, K., Köppen, J., & Kruk, J. W. 2012, A&A, 548, A109

Pages 7 to 18 are available in the electronic edition of the journal at http://www.aanda.org

[16] http://www.esa.int/Our_Activities/Space_Science/Gaia

Table 2. Statistics of the atoms used in our calculations.

Ion		Levels NLTE	Levels LTE	Lines	Ion		Levels NLTE	Levels LTE	Super lines	Sample lines
H	I	15	1	105	Ca	II	7	0	26	2612
	II	1	0	–		III	7	0	28	40 664
He	I	29	74	69		IV	7	0	22	20 291
	II	20	12	190		V	7	0	26	141 956
	III	1	0	–		VI	7	0	26	114 545
C	II	16	30	37		VII	1	0	0	
	III	13	54	32	Sc	II	7	0	26	77 014
	IV	54	4	295		III	7	0	27	687
	V	1	0	0		IV	7	0	26	15 024
N	II	15	232	18		V	7	0	24	261 235
	III	34	32	129		VI	7	0	26	237 271
	IV	16	78	30		VII	1	0	0	
	V	54	8	297	Ti	II	7	0	27	312 054
	VI	1	0	0		III	7	0	25	46 707
O	II	16	31	26		IV	7	0	27	1000
	III	54	18	222		V	7	0	26	26 654
	IV	18	76	39		VI	7	0	26	95 448
	V	19	107	40		VII	1	0	0	
	VI	1	0	0	V	II	7	0	27	734 478
Si	III	17	17	28		III	7	0	25	460 038
	IV	16	7	44		IV	7	0	25	37 130
	V	25	0	59		V	7	0	26	2123
	VI	1	0	0		VI	7	0	25	35 251
P	IV	15	36	9		VII	1	0	0	
	V	18	7	12	Cr	II	7	0	27	728 080
	VI	1	0	0		III	7	0	27	1 421 382
S	III	21	210	35		IV	7	0	24	234 170
	IV	17	83	32		V	7	0	26	43 860
	V	39	71	107		VI	7	0	23	4406
	VI	12	25	25		VII	1	0	0	
	VII	1	0	0	Mn	II	7	0	27	136 814
Zn	III	1	12	0		III	7	0	27	1 668 146
	IV	1	75	0		IV	7	0	25	719 387
	V	94	63	785		V	7	0	25	285 376
	VI	1	0	0		VI	7	0	24	70 116
Ge	III	1	15	0		VII	1	0	0	
	IV	8	1	8	Fe	II	7	0	27	531 170
	V	29	56	119		III	7	0	27	537 689
	VI	1	0	0		IV	7	0	27	3 102 371
						V	7	0	25	3 266 247
						VI	7	0	22	991 935
						VII	1	0	0	
					Co	II	7	0	27	593 140
						III	7	0	27	1 325 205
						IV	7	0	27	552 916
						V	7	0	27	1 469 717
						VI	7	0	25	898 484
						VII	1	0	0	
					Ni	II	7	0	27	322 269
						III	7	0	26	1 033 920
						IV	7	0	27	2 512 561
						V	7	0	27	2 766 664
						VI	7	0	27	7 408 657
						VII	1	0	0	
				Total	19	93	1021	1435	3958	35 286 864

Notes. In the case of iron-group elements (Ca–Ni), the super-lines include the sample lines (Kurucz's LIN lines, cf. Rauch & Deetjen 2003).

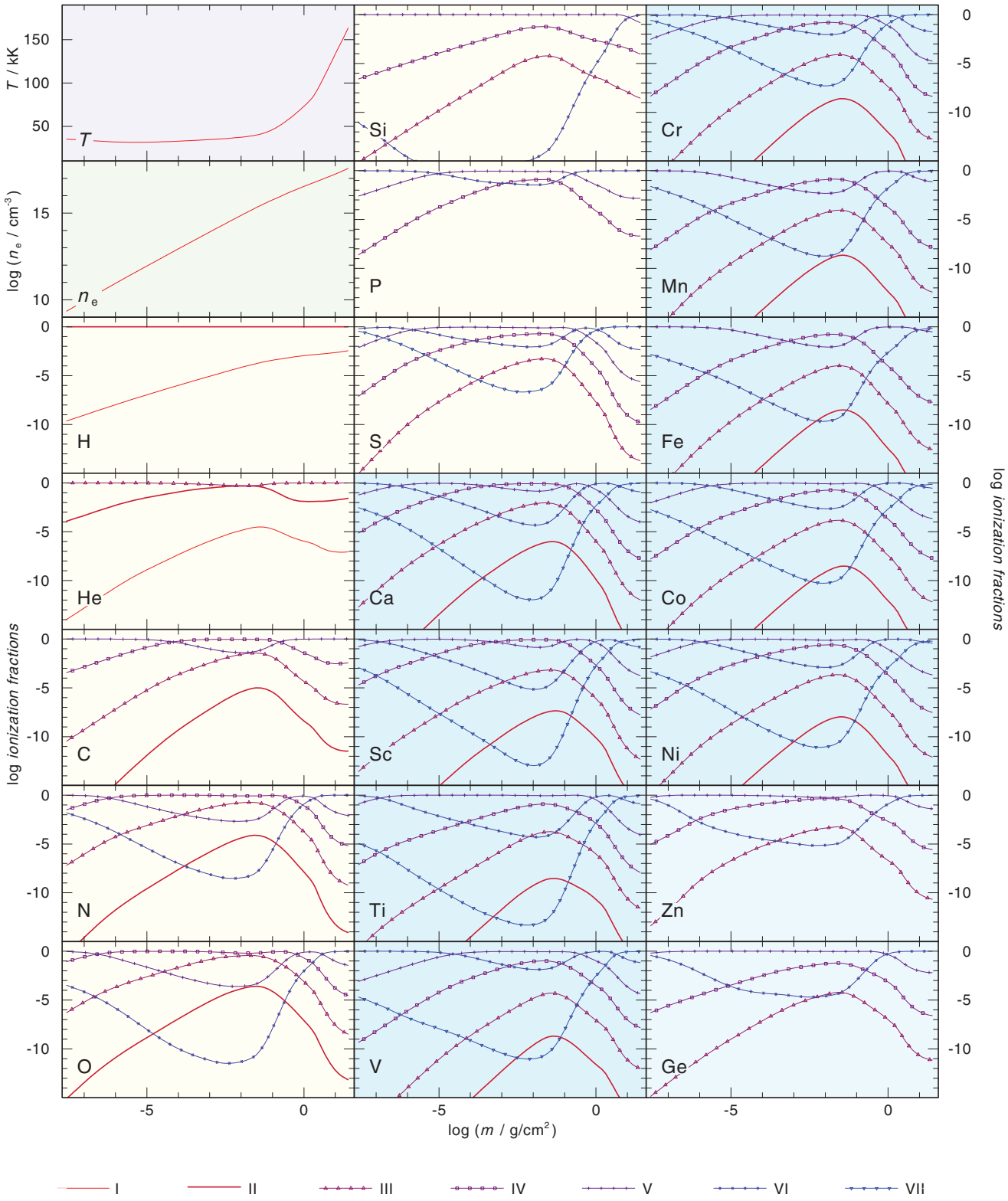

Fig. 3. Temperature and density structure and ionizations fractions of our final model with $T_{\rm eff}$ = 47 250 K and log g = 6.00; m is the column mass, measured from the outer boundary of our model atmosphere.

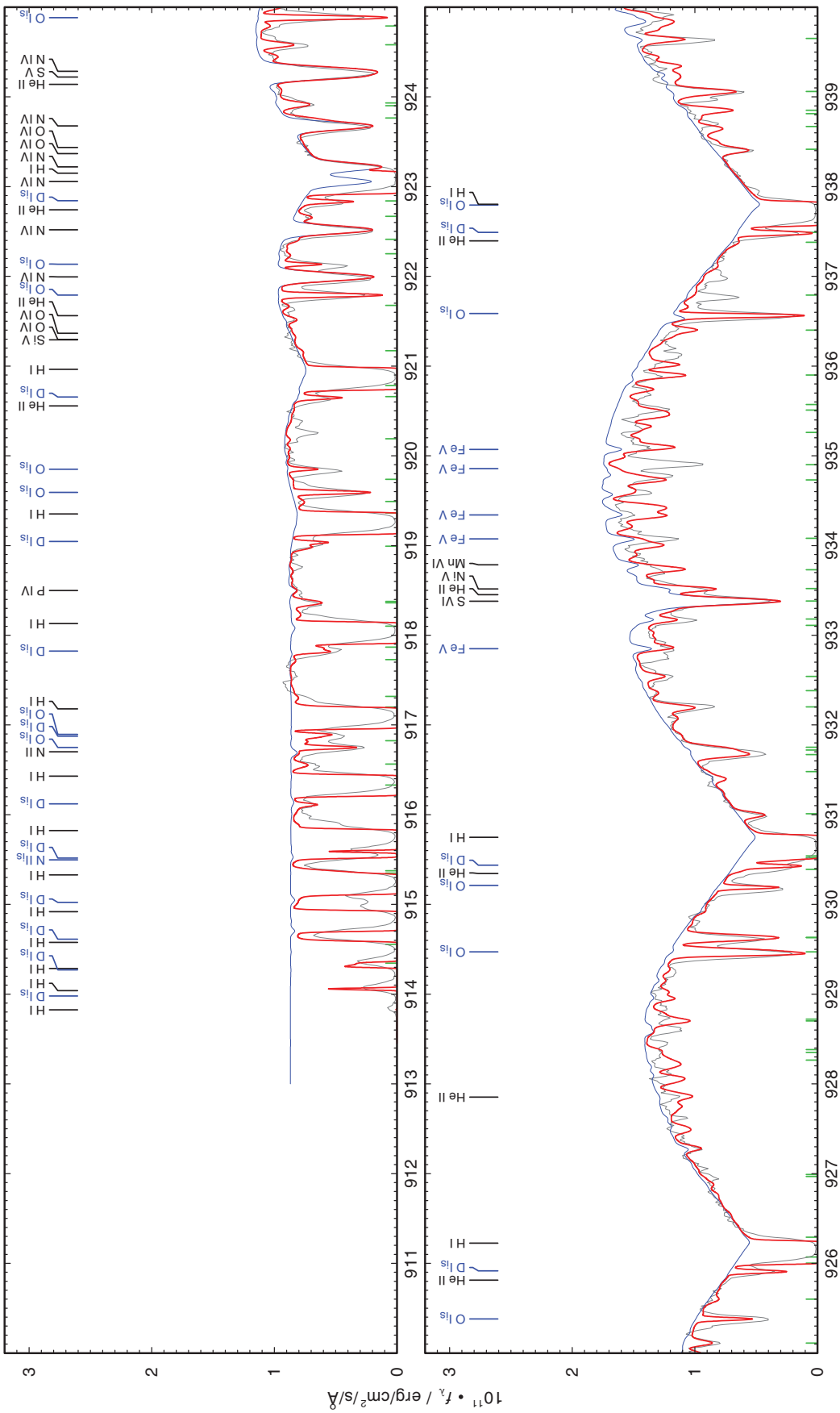

Fig. 7. FUSE spectrum of Feige 110 (gray) compared with synthetic spectra calculated from our final model (red: Kurucz's LIN lines and interstellar line absorption, blue: Kurucz's POS lines). The locations of the strongest stellar (marked in black, Fe and Ni which have the most lines are marked in blue and green for clarity, respectively, for Ca–Ni, only Kurucz's POS lines are identified) and interstellar (marked in blue, with subscript "is") lines are indicated at the top of the panels. The small, green identification marks at the bottom of the panels indicate the locations of interstellar H_2 lines.

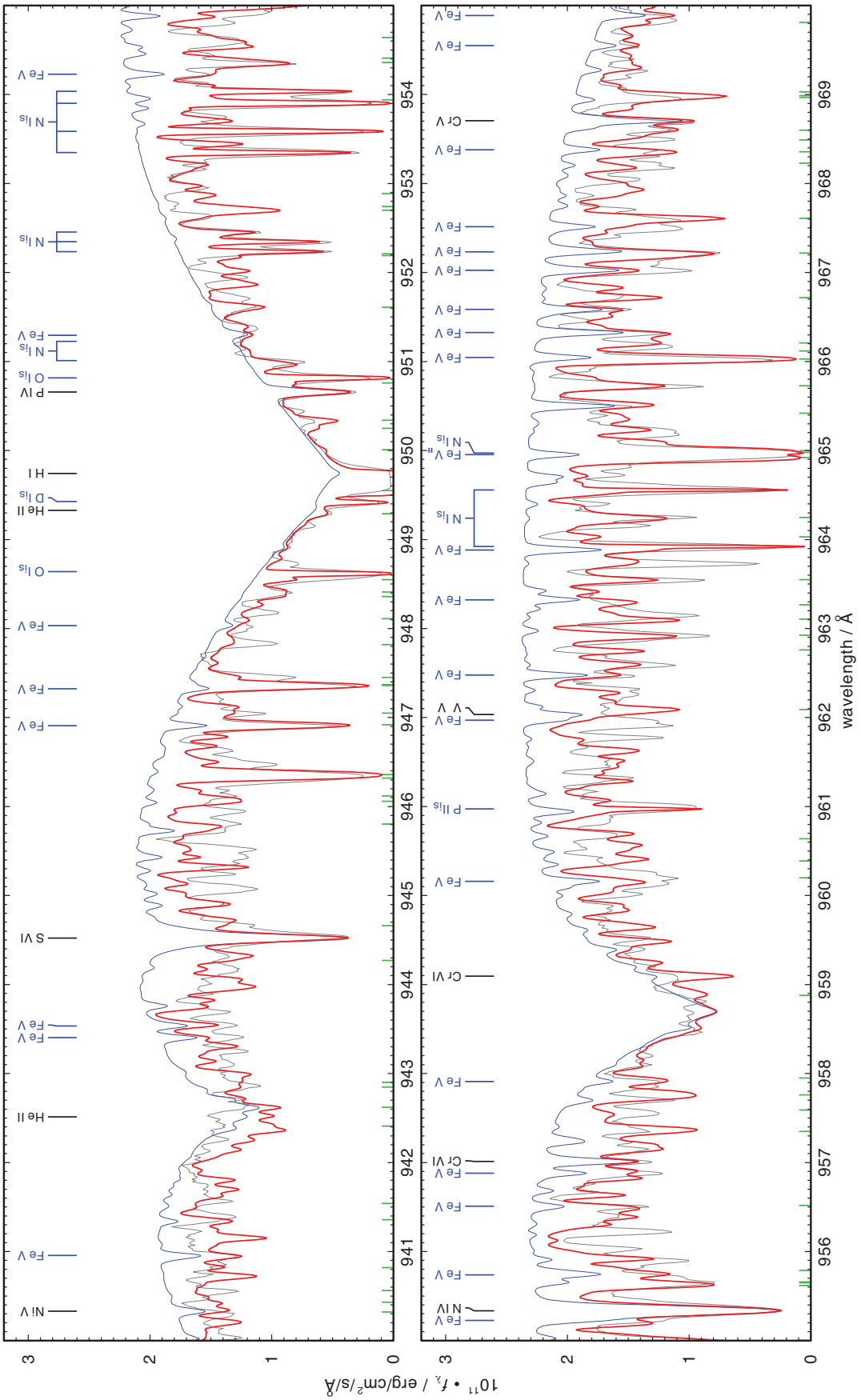
Ni V
Fe V
He II
Fe V
Fe V
S VI
Fe V
Fe V
O I$_{IS}$
He II
D I$_{IS}$
H I
P IV
O I$_{IS}$
N I$_{IS}$
Fe V
N I$_{IS}$
Fe V
N I$_{IS}$
Fe V
Fe V
Fe V

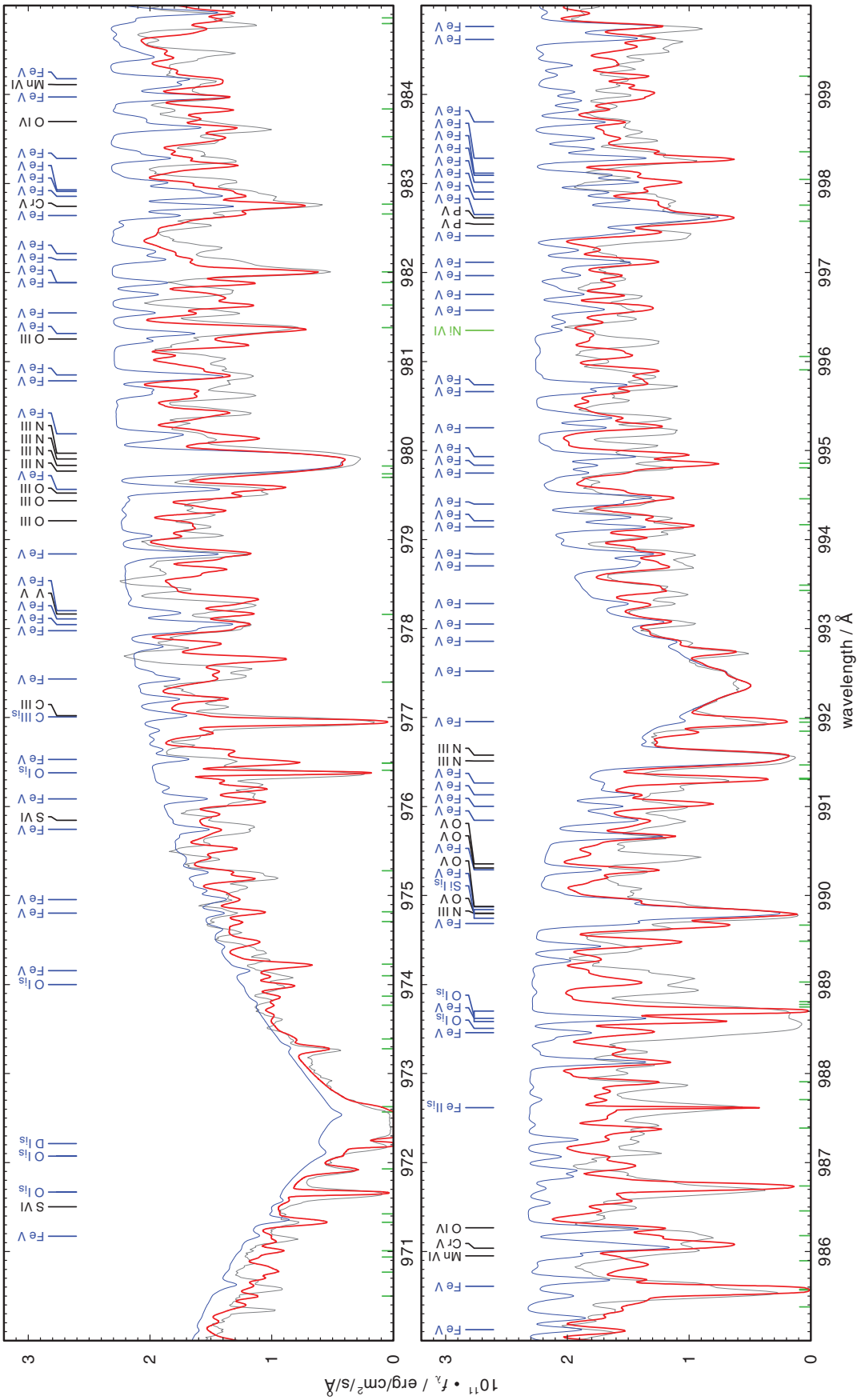

Fig. 7. continued.

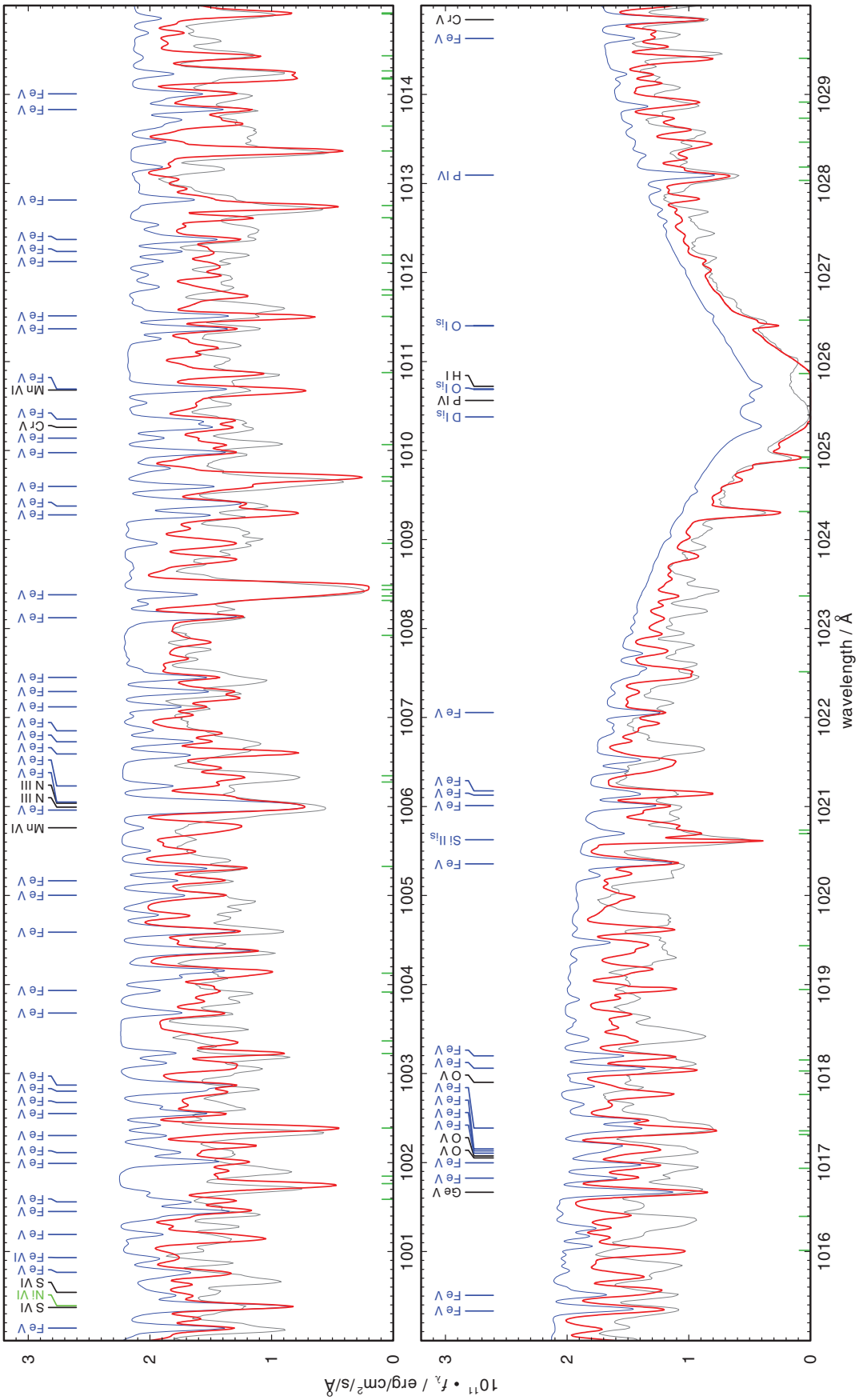

Fig. 7. continued.

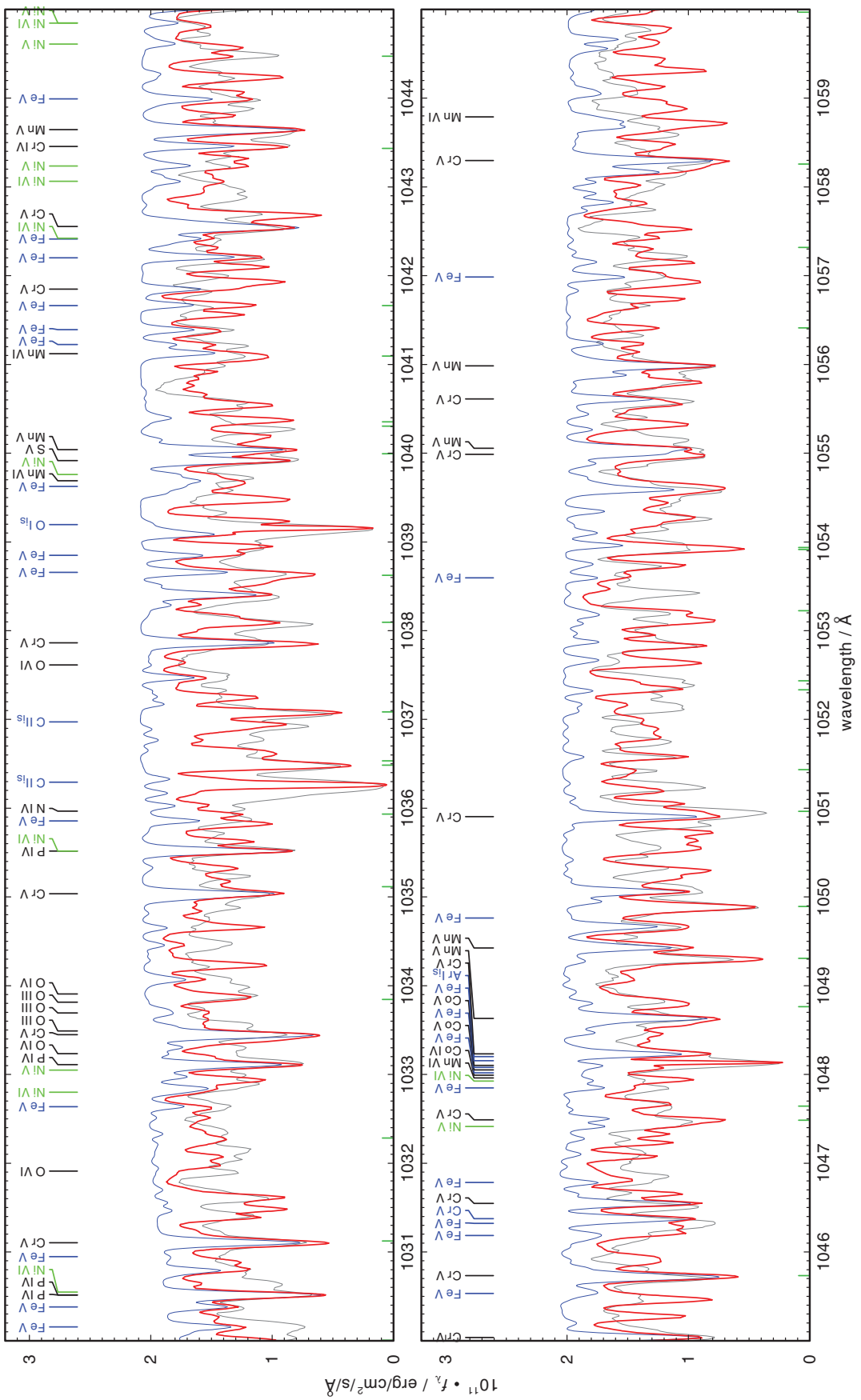

Fig. 7. continued.

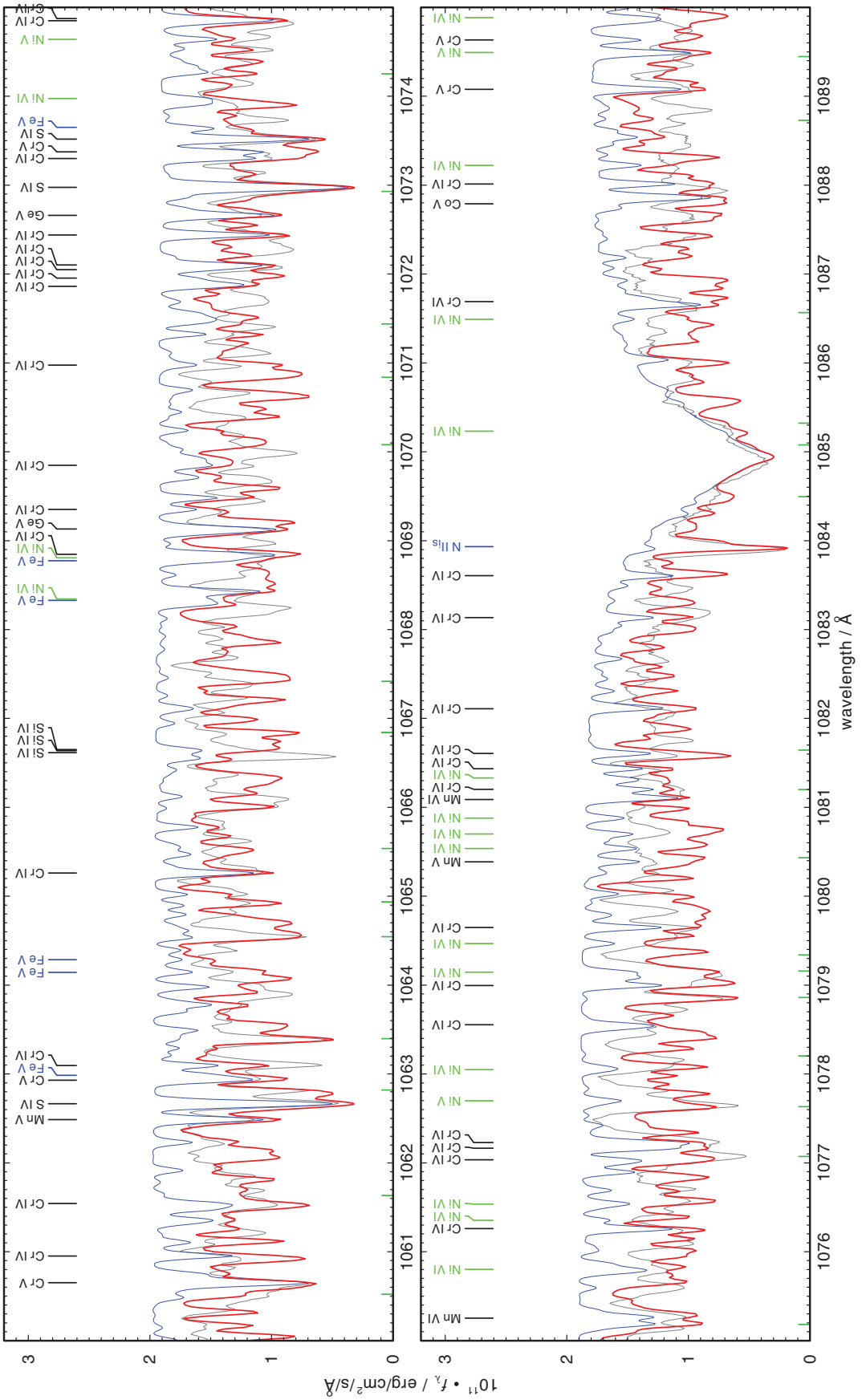

Fig. 7. continued.

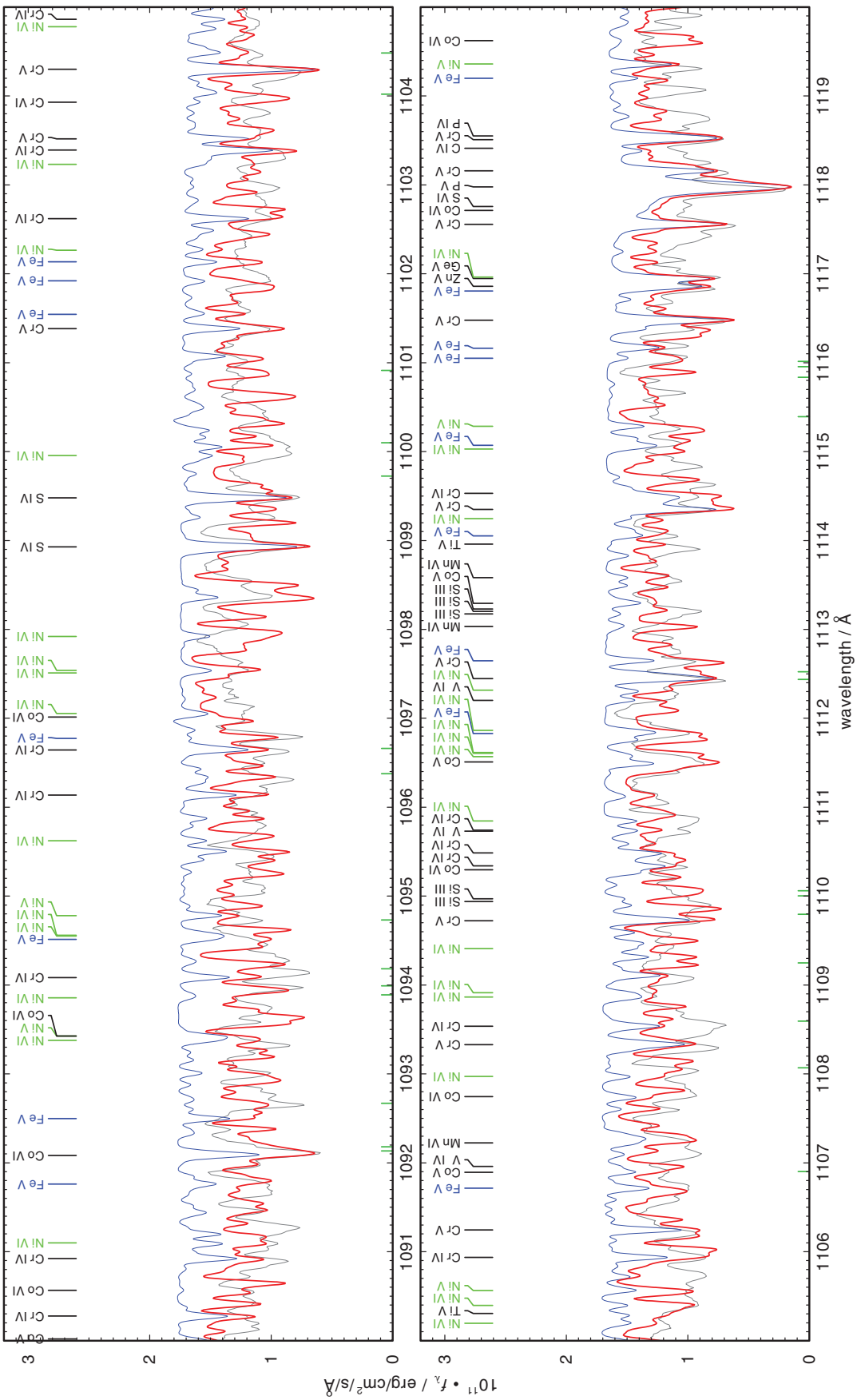

Fig. 7. continued.

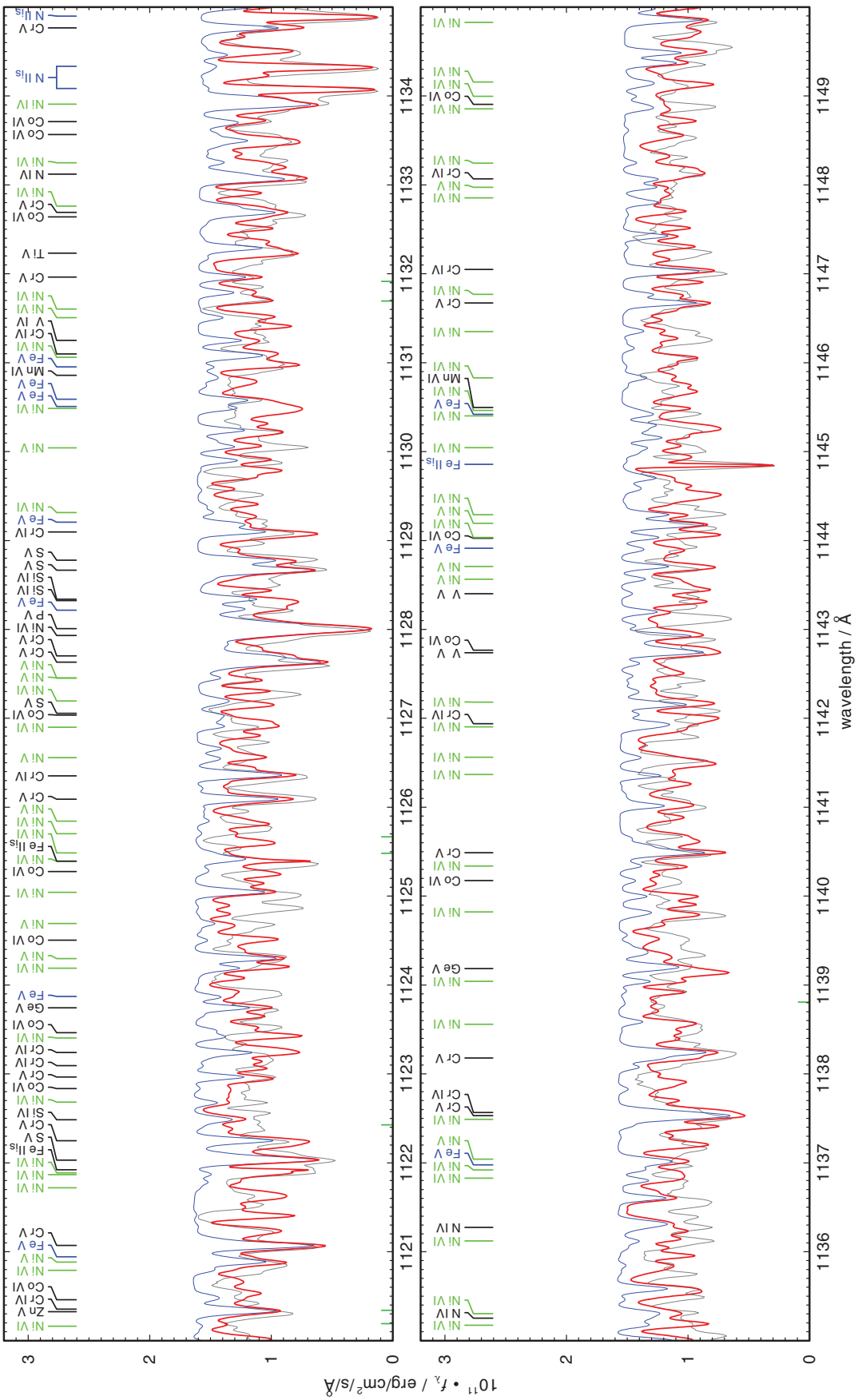

Fig. 7. continued.

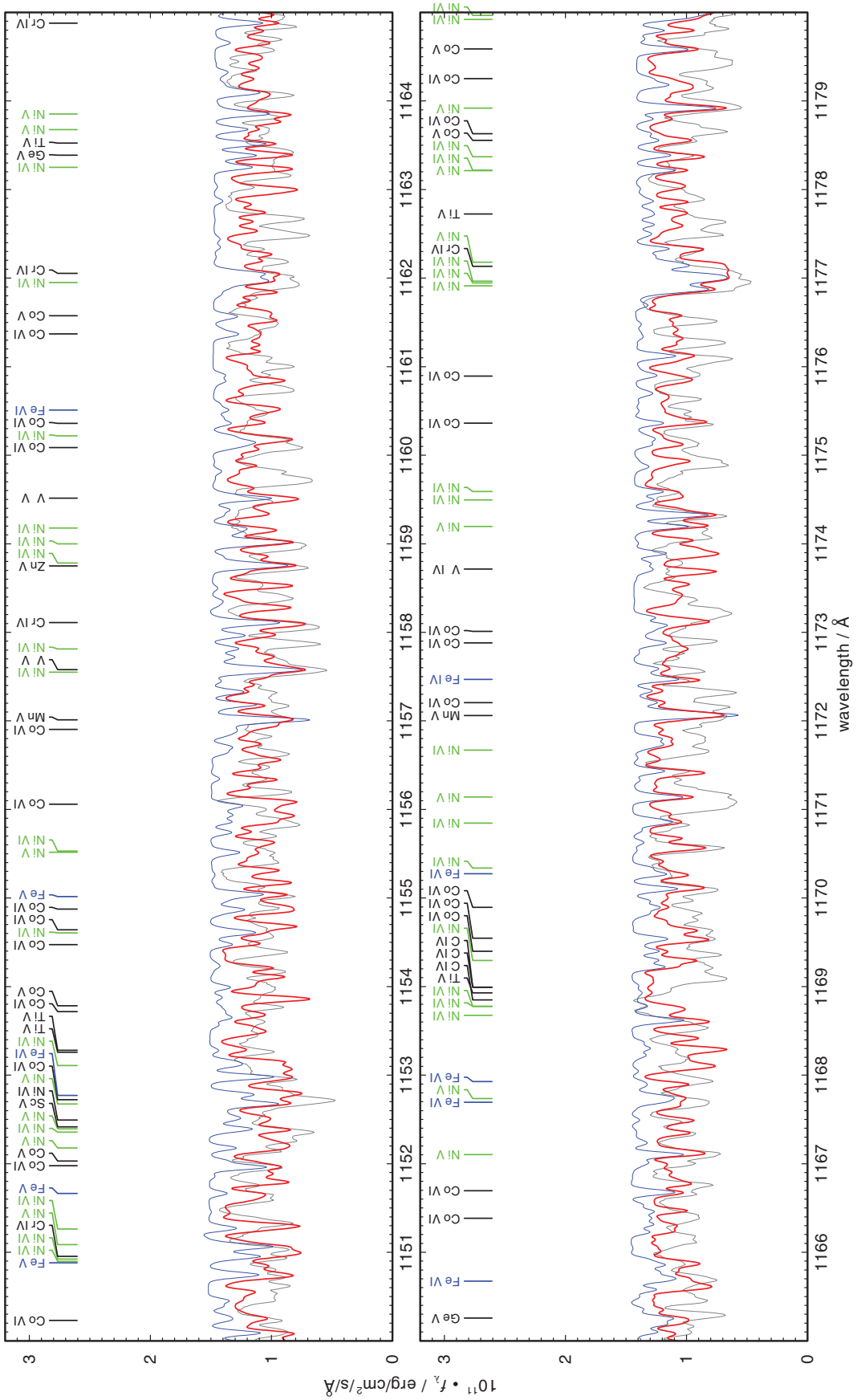

Fig. 7. continued.

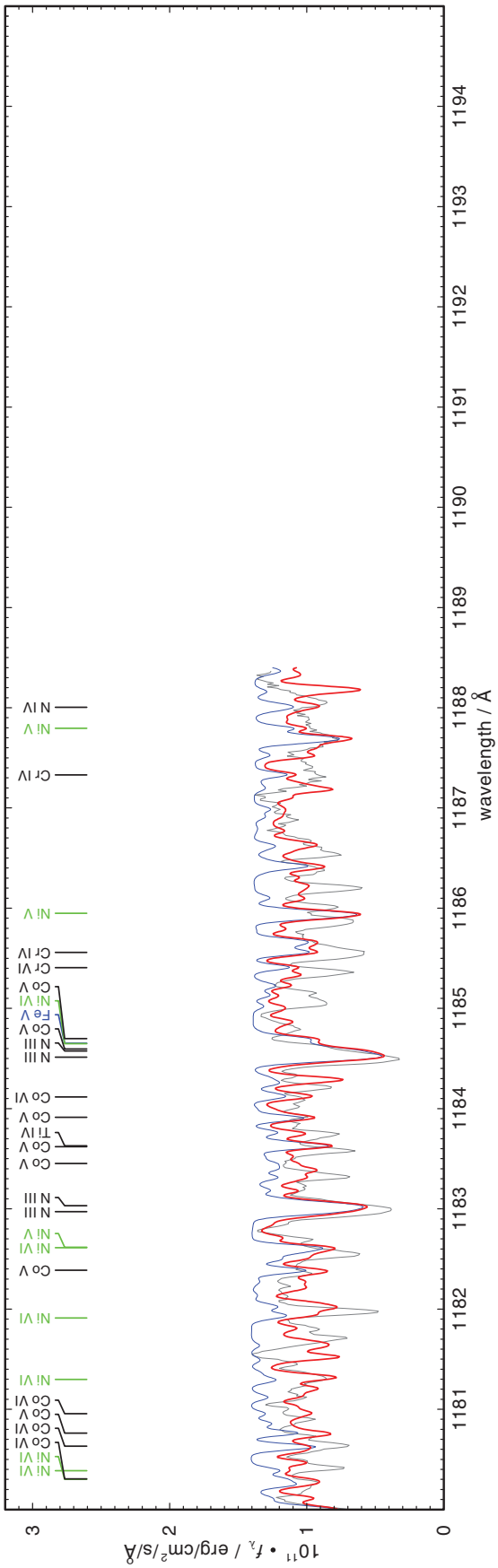

Fig. 7. continued.